Freestanding van der Waals Heterostructures of Graphene and Transition Metal Dichalcogenides

Amin Azizi,[†,‡] Sarah Eichfeld,[†,‡] Gayle Geschwind,[§] Kehao Zhang,[†,‡] Bin Jiang,[∥] Debangshu Mukherjee,[†,‡] Lorraine Hossain,[†] Aleksander F. Piasecki,[†] Bernd Kabius,[‡] Joshua A. Robinson,[*,†,‡] and Nasim Alem[*,†,‡]

[†]Department of Materials Science and Engineering and Center for Two Dimensional and Layered Materials and [‡]Materials Research Institute, The Pennsylvania State University, University Park, Pennsylvania 16802, United States, [§]Department of Physics and Astronomy, Stony Brook University, Stony Brook, New York 11794-3800, United States, and [∥]FEI Company, 5350 NE Dawson Creek Drive, Hillsboro, Oregon 97124, United States

ABSTRACT Vertical stacking of two-dimensional (2D) crystals has recently attracted substantial interest due to unique properties and potential applications they can introduce. However, little is known about their microstructure because fabrication of the 2D heterostructures on a rigid substrate limits one's ability to directly study their atomic and chemical structures using electron microscopy. This study demonstrates a unique approach to create atomically thin freestanding van der Waals heterostructures—WSe_2/graphene and MoS_2/graphene—as ideal model systems to investigate the nucleation and growth mechanisms in heterostructures. In this study, we use transmission electron microscopy (TEM) imaging and diffraction to show epitaxial growth of the freestanding WSe_2/graphene heterostructure, while no epitaxy is maintained in the MoS_2/graphene heterostructure. Ultra-high-resolution aberration-corrected scanning transmission electron microscopy (STEM) shows growth of monolayer WSe_2 and MoS_2 triangles on graphene membranes and reveals their edge morphology and crystallinity. Photoluminescence measurements indicate a significant quenching of the photoluminescence response for the transition metal dichalcogenides on freestanding graphene, compared to those on a rigid substrate, such as sapphire and epitaxial graphene. Using a combination of (S)TEM imaging and electron diffraction analysis, this study also reveals the significant role of defects on the heterostructure growth. The direct growth technique applied here enables us to investigate the heterostructure nucleation and growth mechanisms at the atomic level without sample handling and transfer. Importantly, this approach can be utilized to study a wide spectrum of van der Waals heterostructures.

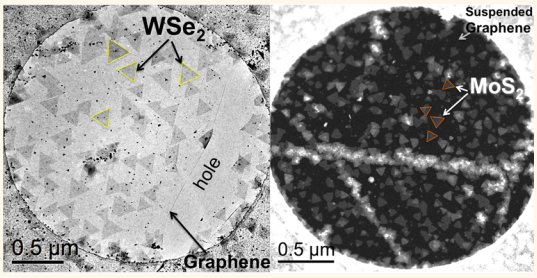

KEYWORDS: freestanding heterostructures · transmission electron microscopy · transition metal dichalcogenides · graphene · atomic and chemical structure · MoS_2 · WSe_2

Beyond research on graphene-like crystals,[1−4] creation of vertically stacked van der Waals heterostructures has recently gained great interest[5−9] due to their unique properties and potential applications in electronic and optoelectronic devices[6−8,10,11] and superconductors with high critical temperature (T_C).[5] Transition metal dichalcogenides (TMDs), such as tungsten diselenide (WSe_2) and molybdenum disulfide (MoS_2), are considered active and efficient catalysts for hydrogen evolution reaction (HER) by both theory[12,13] and experiment.[14,15] Moreover, edge sites in WSe_2 and MoS_2 are electrocatalytically active.[12,15,16] Therefore, WSe_2/graphene and MoS_2/graphene heterostructures with large surface area, a high density of edge states, and a conductive single-layer graphene support could be a promising electrocatalyst for HER. Vertical heterostructures have been realized through isolation of single-layer flakes by exfoliation[7,17−20] or growth of the layered structures on a substrate[21−25] followed by transferring and stacking. Interface contamination due to manual stacking of layers is an important problem that can deteriorate the performance of the heterostructures.[5,26] To mitigate this issue, direct growth of heterolayers on different substrates has also been achieved.[26,27] These approaches have been successful in measuring the resulting electronic and optoelectronic properties of heterostructures but have been very limiting in allowing us to image and probe the atomic registry, interfacial structure, and chemistry of heterostructures. Understanding the atomic and

* Address correspondence to alem@matse.psu.edu, jrobinson@psu.edu.

Received for review November 10, 2014 and accepted April 17, 2015.

Published online April 17, 2015
10.1021/acsnano.5b01677

chemical structure of heterostructures is the key to probe the competing physics and chemistry at the nanoscale and to further tune their properties. Here, we report a unique approach to create atomically thin freestanding heterostructures with minimal contamination. This approach allows us to probe the atomic structure and chemistry of the heterostructures directly after the growth and also to study the nucleation and growth at different stages. In addition, photoluminescence (PL) and Raman studies here present a unique example on how a substrate can tune the optoelectronic properties of a heterostructure. We utilize a combination of transmission electron microscopy (TEM) imaging and selected area electron diffraction (SAED) to study commensurability in the grown WSe_2/graphene and MoS_2/graphene heterostructures. Aberration-corrected scanning transmission electron microscopy (STEM) and energy-dispersive X-ray spectroscopy (EDS) are used to study the atomic and chemical structure of the WSe_2/graphene and MoS_2/graphene heterostructures, while optical spectroscopy determines their resulting optical properties. We also show how graphene defects and grain boundaries can promote heterostructure growth and lead to the formation of multilayer flakes. Importantly, the process presented here can readily be translated to other van der Waals heterostructures and opens up a new paradigm in atomic-scale characterization of these novel materials.

RESULTS AND DISCUSSION

Figure 1a presents schematics of the fabrication process of the freestanding vertical heterostructures. Graphene was first grown on a Cu substrate *via* chemical vapor deposition (CVD)[1] and then transferred to a Quantifoil TEM grid with 2 μm holes. Here, we used a direct polymer-free process to transfer large-area graphene to the holey carbon grid (see details in the Experimental Section).[28] The TEM image and its corresponding selected area diffraction pattern in Figure 1b confirm a suspended graphene film uniformly covering the TEM grid prior to synthesis of heterostructures. We use the suspended graphene substrate on the TEM grid for direct growth of TMD structures. The monolayer WSe_2 and MoS_2 triangles were grown on the graphene grids *via* metal organic chemical vapor deposition (MOCVD)[29] and oxide powder vaporization, respectively. WSe_2 flakes can be seen in Figure 1c as dark triangles evenly dispersed on freestanding graphene with a lateral size of 100−400 nm. The triangles are orientated only in two opposing directions, strongly suggesting the presence of a strict crystallographic orientation relationship between WSe_2 and its graphene substrate. Additionally, each triangle is equilateral with a 60° angle, suggesting that they are single-crystal.[30] Figure 2a depicts two WSe_2 triangles oriented in opposite directions. SAED of the large triangle (yellow dashed circle in Figure 2a) confirms the single-crystal nature of both WSe_2 and the underlying graphene layer and their preferred orientation relationship (Figure 2b). The yellow dashed line in Figure 2b indicates that the single-layer WSe_2 and the freestanding graphene substrate exhibit the same orientation, verifying epitaxial growth of WSe_2 on the graphene membrane. We performed diffraction analysis on more than 40 WSe_2 triangles to statistically determine the relative orientation of the WSe_2 and graphene lattices (Figure 2c). A significant fraction of single-layer WSe_2 triangles are epitaxially grown on graphene, while a low misorientation angle is found between a few WSe_2 triangles and graphene potentially due to the existence of graphene wrinkles and/or surface contamination. Figure 2d presents the top and side views of the structural schematics for the WSe_2/graphene vertical heterostructure. WSe_2 has a layered structure with a trigonal symmetry and a lattice constant of 3.28 Å, in which a triangular lattice of tungsten (W) atoms is located between two triangular lattices of selenium (Se) atoms. Within a monolayer, W and Se atoms are bonded together by strong covalent bonds, while the neighboring layers show interlayer coupling through van der Waals interactions. Graphene, on the other hand, has a hexagonal symmetry with a lattice constant of 2.46 Å. A heterostructure of WSe_2/graphene consequently has a lattice mismatch of about 33% between graphene and WSe_2. Despite this large lattice mismatch, we observe WSe_2 to grow epitaxially on graphene. This reveals that the 2D layered crystals can grow epitaxially as a result of weak van der Waals forces and the absence of dangling bonds between layers.[31,32] Such weak interlayer characteristics provide a route for the crystal to yield a commensurate growth between highly mismatched materials through van der Waals epitaxy.[33] Through diffraction analysis (Figure 2b), the reciprocal lattice vectors (g vectors) for WSe_2 and graphene were analyzed, giving a ratio of ~0.75, which corresponds to the inverse ratio of their lattice spacing. This analysis provides evidence that every third W atom sits nearly perfectly above every fourth C atom along the zigzag direction in WSe_2/graphene heterostructure. The structural model of the WSe_2/graphene heterostructure with circled W atoms nearly perfectly above C atoms along the zigzag direction (six directions shown in Figure 2d) confirms the diffraction results. By connecting the marked W atoms along the zigzag direction, aligned equilateral triangles form, oriented either up or down. The smallest triangles have a lateral size of about 9.84 Å (3 and 4 times the WSe_2 and graphene lattice constants, respectively), which is in agreement with the diffraction pattern. As seen in the configuration shown in Figure 2d, many W atoms (less than 1 nm apart) superimpose on the C atoms, suggesting that an energy minima may exist between the two layers when aligned in this manner.

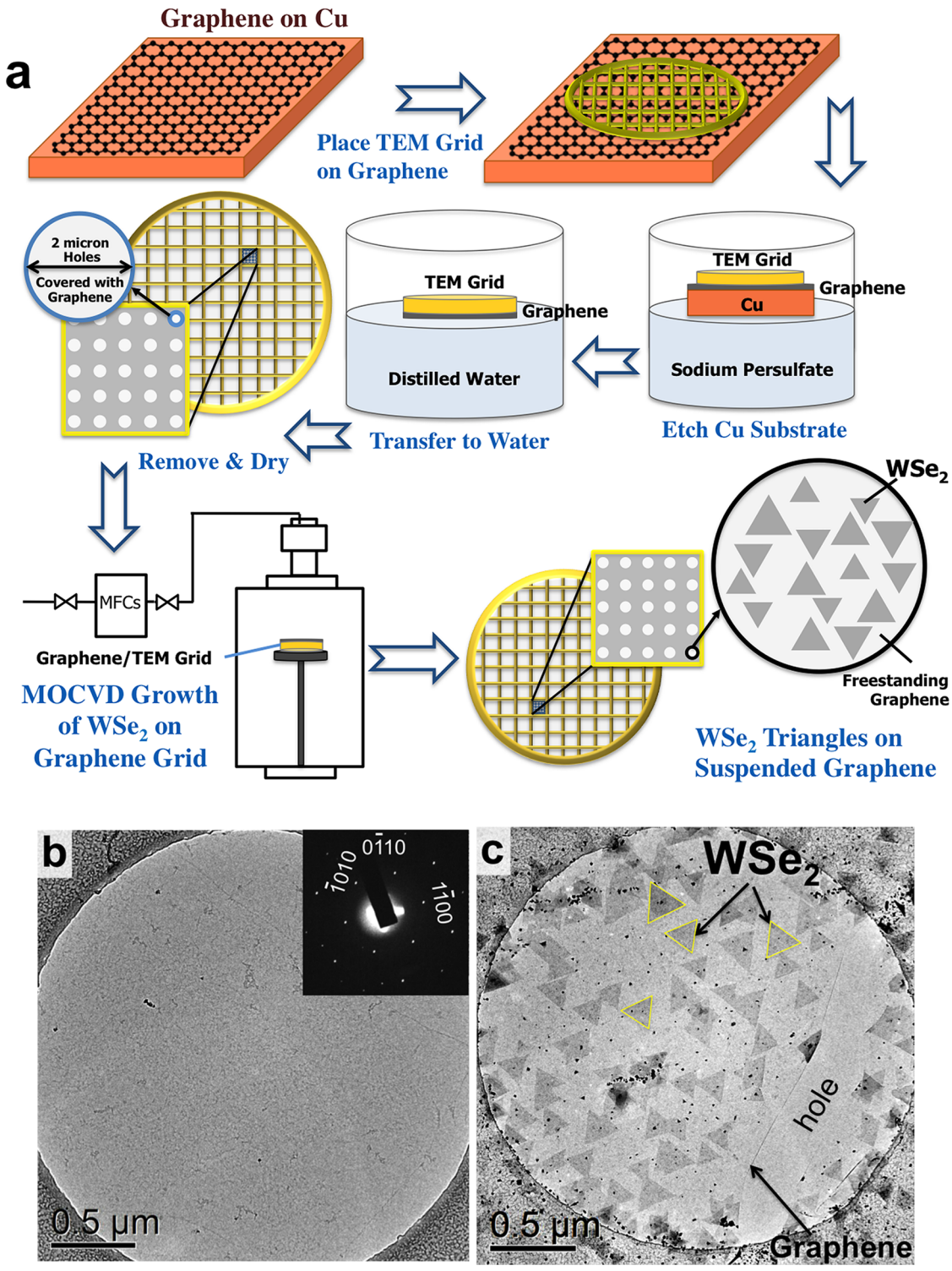

Figure 1. (a) Schematics of the fabrication process of the WSe_2/graphene heterostructure. Graphene grown on Cu was directly transferred to a Quantifoil TEM grid with 2 μm holes using a polymer-free transfer process. The monolayer WSe_2 triangles were directly grown on the large-area suspended graphene membrane through MOCVD. TEM images showing (b) single-layer graphene sheet covering a TEM grid hole before heterostructure growth and (c) WSe_2 triangles epitaxially grown on the freestanding graphene membrane.

Figure 3a shows annular dark-field scanning transmission electron microscopy (ADF-STEM) image of the WSe_2/graphene heterostructure. The WSe_2 triangles can be clearly seen in this figure. While most of the triangles are monolayer, few triangles with multiple layers are also observed. Regions that exhibit multilayer growth are oriented with no misorientation with respect to the bottom WSe_2 layer (Figure 3a), indicating that each subsequent layer is also epitaxial. High-angle annular dark-field (HAADF)-STEM image shown in

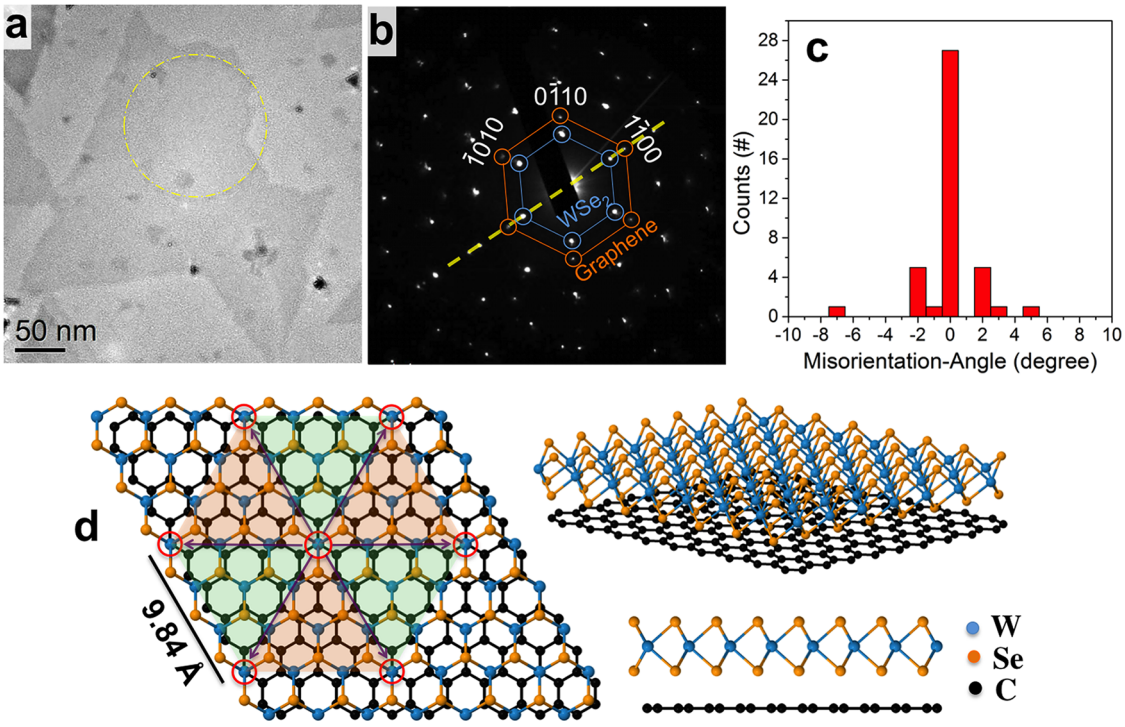

Figure 2. (a) TEM image indicating two WSe_2 triangles with opposite orientations. (b) Selected area electron diffraction pattern taken from the larger triangle (indicated with the yellow dashed circle in panel a). (c) Histogram of misorientation angle of WSe_2 triangles grown on the suspended graphene, confirming the epitaxial growth of the majority of the triangles on graphene. (d) Top and side view structural models of the WSe_2/graphene vertical heterostructure.

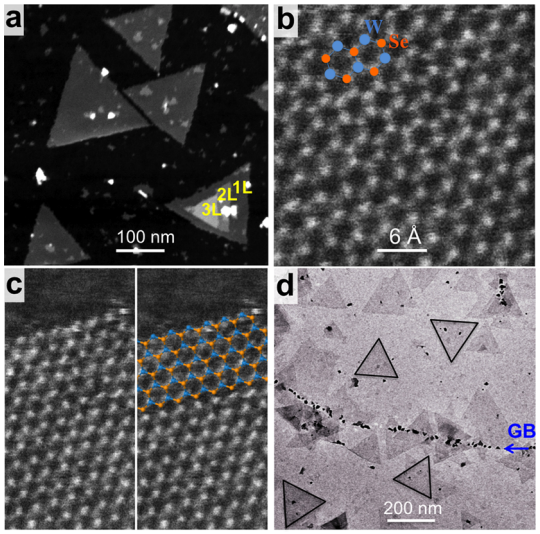

Figure 3. (a) HAADF-STEM image of the WSe_2 triangles on the graphene support. The lower right triangle reveals monolayer, bilayer, and trilayer regions. (b) HAADF-STEM image of a monolayer WSe_2, showing the W atoms and two Se atoms as bright and dim spots, respectively. (c) HAADF-STEM image of the edge of a WSe_2 triangle showing a W-terminated zigzag edge. (d) TEM image of WSe_2/graphene heterostructure showing the presence of a graphene grain boundary and its impact on WSe_2 growth.

Figure 3b indicates a region of the monolayer WSe_2 where the atomic structure is resolved and W and Se atoms can be distinguished. Since the intensity of HAADF-STEM images depends on the atomic number, W exhibits higher contrast while Se columns are slightly dimmer spots.[34] The atomic-resolution HAADF-STEM image from the edge of a WSe_2 triangle shows zigzag edges with W atom termination (Figure 3c). Zigzag edges are predicted to be the energetically preferred structure for TMDs with triangular morphology.[35]

Defects in the substrate can have a profound effect on the nucleation and growth of heterostructures. Dangling bonds at grain boundaries, defects, and curved sp^2 π-bonds at wrinkles are more reactive and can attract adsorbates.[26,27,31,32] Figure 3d and Supporting Information Figure S1 show TEM images of a graphene grain boundary acting as the nucleation sites for the growth of the heterostructure. The two groups of triangles on different sides of the line defect are aligned in two different orientations, while a high density of small triangles and particulates along the boundary suggests the high reactivity of the line defect. Diffraction analysis verifies the existence of two grains with different orientations and consequently the presence of a grain boundary in the graphene membrane (Figure S1c–e). Evident from TEM, the quality of suspended graphene has a significant impact on heterostructure growth, and the formation of multilayer flakes and 3D particulates is favorable on graphene defects.

(Scanning) transmission electron microscopy images of the heterostructure also indicate deposition

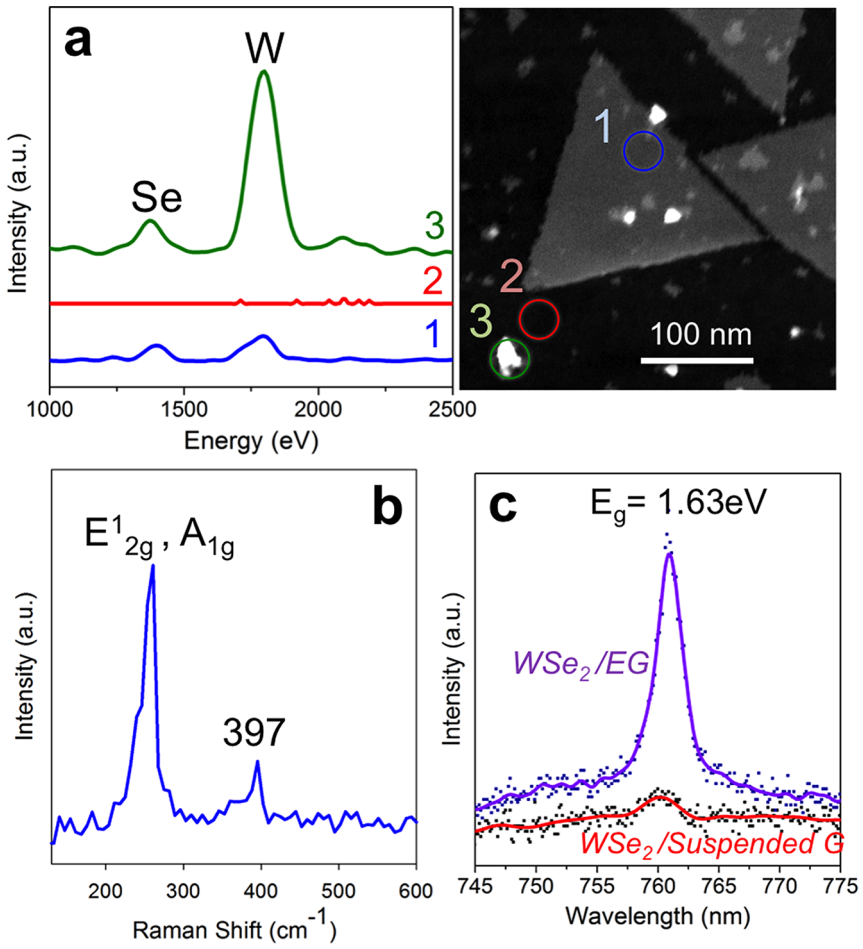

Figure 4. (a) Line-scan energy-dispersive X-ray spectroscopy and (b) Raman spectrum obtained from the freestanding WSe_2/graphene heterostructure. (c) Photoluminescence spectra acquired from the suspended WSe_2/graphene and a WSe_2/EG heterostructures (the scatter and line plots indicate the real and smoothed data, respectively). The EDS spectra from neighboring regions marked in the top-right HAADF-STEM image (blue, red, and green) reveal the tungsten-rich nature of the particulates. The Raman peaks at 258 and 397 cm^{-1} correspond to E^1_{2g}/A_{1g} vibrational modes and the second-order modes of the WSe_2 monolayers, respectively. PL spectra reveal more severe quenching in the freestanding WSe_2/graphene heterostructure compared with the WSe_2/EG.

of particulates on graphene during the growth (Figures 1c and 3a). EDS in the STEM mode has been performed to probe the chemical nature of the particulates. Figure 4a shows three EDS spectra from neighboring regions marked in the right HAADF-STEM image: WSe_2 on graphene (blue), graphene (red), and a particulate on graphene (green). A much higher ratio of W/Se is observed for the particulate compared with the WSe_2 triangle, indicating that the particulates are W-rich. Raman spectroscopy and PL measurements were performed directly on the suspended WSe_2/graphene heterostructure to further study the structure of the WSe_2 triangles grown on suspended graphene. Figure 4b shows the Raman spectrum of the WSe_2 triangles on a monolayer graphene membrane. The two peaks observed in Raman correlate with those identified for WSe_2.[36,37] The peak at 258 cm^{-1} corresponds to both the in-plane and out-of-plane (E^1_{2g} and A_{1g}, respectively) vibrational modes of the WSe_2 monolayers,[36] while the peak at 397 cm^{-1} and the shoulder on its left can be assigned to the second-order modes.[37] The PL spectrum of the monolayer WSe_2 triangles on freestanding graphene can be seen in Figure 4c, showing an emission at 760 nm as a signature of monolayer WSe_2. The PL has been significantly quenched compared to WSe_2 on epitaxial graphene (EG) with a comparable average size and thickness (see Supporting Information Figure S2 for the AFM image and Raman spectrum of the WSe_2/EG sample). Photoluminescence quenching has been also observed in other heterostructures involving graphene due to photogenerated charge carriers transferring from the TMD layer to graphene.[21,36] The severity of quenching is believed to be due to the absence of a bulk and rigid substrate that can lead to improved efficiency in graphene's ability to transport carriers away from the WSe_2.

This study also investigates nucleation and growth of MoS_2 on freestanding graphene synthesized *via* oxide powder vaporization. Figure 5a presents the

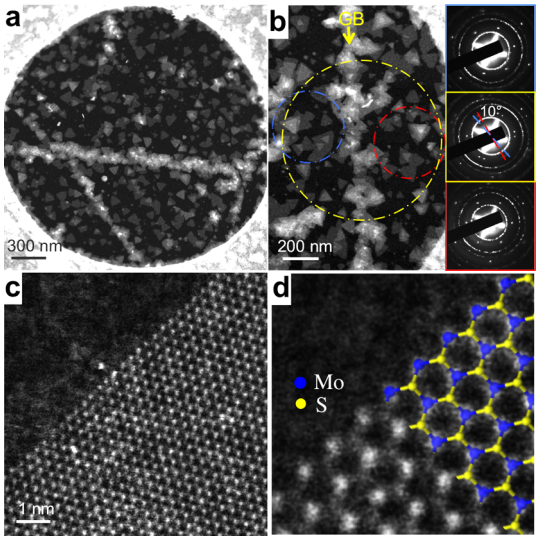

Figure 5. (a) HAADF-STEM image of the MoS_2/suspended graphene heterostructure. (b) HAADF/STEM image and SAED patterns of the heterostructure with a line defect in the graphene support. The graphene grain boundary acts as the nucleation sites for the growth of MoS_2 and formation of multilayer flakes. (c) Atomic-resolution HAADF-STEM image showing the edge structure of the MoS_2 triangles grown on the suspended graphene. (d) Magnified image of the atomic-resolution image overlaid with the MoS_2 structural model, indicating a metal-terminated zigzag edge for the MoS_2 triangles.

HAADF-STEM image of the grown MoS_2 triangles on the suspended graphene membrane. MoS_2 monolayers are seen as dark-gray equilateral triangles, while multilayer regions exhibit higher contrast and freestanding single-layer graphene displays black color. The triangles are monocrystalline with the average size of ~100 nm. Interestingly, the MoS_2 triangles are orientated in random directions, indicating the non-epitaxial growth of MoS_2 on graphene, potentially resulting from different growth conditions (*i.e.*, lower growth temperature) and/or different materials systems. Further study is needed to better understand the origin of the epitaxial growth in these heterostructure systems. A high density of MoS_2 triangles can be seen along the graphene grain boundaries, similar to the WSe_2/graphene heterostructures. Figure 5b shows a HAADF/STEM image and SAED patterns of a 10° graphene grain boundary that acts as the nucleation sites for the growth of MoS_2. The SAED pattern from the area indicated by the yellow circle shows two sets of diffraction spots for graphene, presenting the existence of two graphene grains. The SAED patterns from the left (blue) and right (red) of the boundary show only one set of graphene diffraction spots, which indicates the presence of a 10° grain boundary in the graphene membrane. The ring pattern from the MoS_2 lattice also confirms the non-epitaxial nature of the MoS_2 flakes. It is evident from both heterostructures that defects have a higher reactivity for the growth of the TMD heterostructures studied here. Figure 5c shows an atomic-resolution HAADF-STEM image from the edge of a MoS_2 triangle, in which Mo and S exhibit bright and dim contrast, respectively. Figure 5d demonstrates a magnified image of the atomic-resolution image (Figure 5c) overlaid with the MoS_2 structural model. Despite the presence of edge roughness after growth, MoS_2 triangles grown on graphene maintain zigzag edges mostly with a metal-termination configuration, similar to WSe_2 triangles on graphene. To prevent damage in the nanostructures, care should be taken during imaging by choosing a low electron dose for the STEM probe. Beam damage is, in particular, important for the atoms at the edges and defects due to a lower knock-on energy threshold than the bulk. Recent work has shown low-dose imaging to significantly reduce the beam−sample interactions and damage during imaging.[38,39] To avoid sample damage, we have reduced the electron dose in the STEM probe by spreading the beam at the monochromator. However, to further confirm the genuine edge structure of the sample before any possible beam damage, the electron dose can be further reduced.

Energy-dispersive X-ray spectroscopy maps of the MoS_2 triangle (marked in Figure 6a) exhibit the chemical composition of the heterostructure. Figure 6b−d shows EDS elemental maps for C, S, and Mo, indicating a uniform distribution of C in the graphene support, while Mo and S are found locally within the triangular domain. Similar to the case of WSe_2, we performed an electron diffraction study on more than 70 MoS_2 flakes to statistically reveal the orientation relationship between the MoS_2 and graphene lattices. Figure 6e presents the distribution of misorientation angles between MoS_2 and graphene, verifying the non-epitaxial growth and random orientations of MoS_2 triangles on suspended graphene. Raman and PL measurements performed on the freestanding MoS_2/graphene heterostructure show the signature peaks for MoS_2 (Figure 6f,g). The Raman spectrum indicates the E^1_{2g} and A_{1g} peaks, respectively, located at 385 and 404 cm^{-1}. The peak distance of ~19 cm^{-1} between A_{1g} and E^1_{2g} peaks strongly suggests the growth of MoS_2 monolayers,[40] as also observed in the ADF-STEM images. Significant quenching of PL response from MoS_2 can be seen when it is on freestanding graphene compared with sapphire and epitaxial graphene (Figure 6g) (also see Supporting Information Figure S3 for the SEM images and PL and Raman spectra of the MoS_2/EG and MoS_2 on sapphire samples). This photoluminescence quenching is consistent with what is observed for the WSe_2 flakes on the suspended graphene. One can expect a significant reduction in surface optical phonon scattering in the graphene layer when the substrate is removed,[41,42] which would be a source of enhancement in the efficiency of charge carrier collection in the layer and thus quenching of the PL.

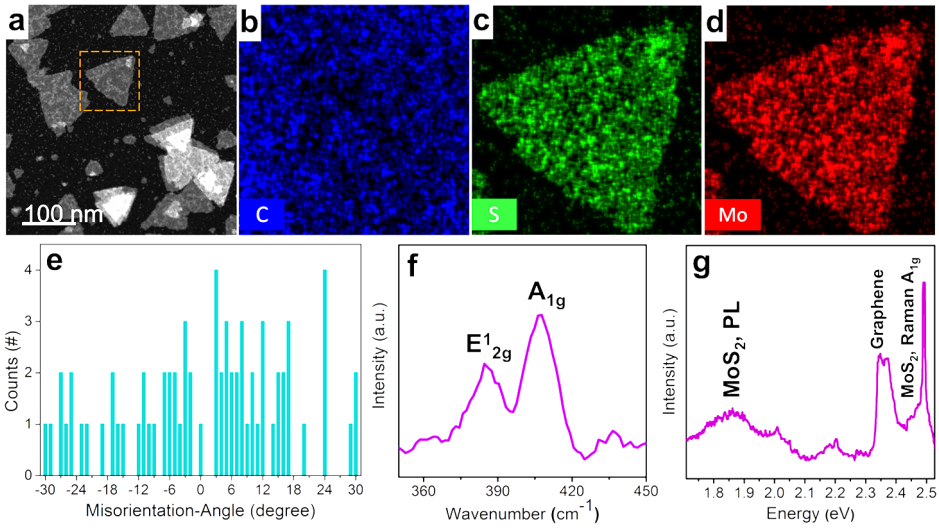

Figure 6. (a) HAADF-STEM image of the MoS_2/graphene heterostructure showing several single- and multilayer triangles. EDS maps of (b) C, (c) S, and (d) Mo, which confirms the homogeneous distributions of carbon in the graphene substrate and sulfur and molybdenum only within the triangle. (e) Histogram of misorientation angle of MoS_2 triangles with respect to graphene, indicating the non-epitaxial growth of MoS_2 on graphene. (f) Raman and (g) PL spectra of the freestanding MoS_2/graphene heterostructure. The Raman peaks located at 385 and 404 cm^{-1} correspond to the E^1_{2g} and A_{1g} modes of MoS_2, respectively. The PL of the MoS_2 on the suspended graphene shows a substantial quenching compared to the MoS_2/sapphire and MoS_2/EG samples (see Supporting Information Figure S3).

CONCLUSIONS

This study presents a novel approach to create atomically thin freestanding van der Waals heterostructures, enabling us to directly probe their atomic structure and chemistry. We have investigated the atomic and chemical structure of two heterostructure systems, WSe_2/graphene and MoS_2/graphene, grown by two different approaches. We observe epitaxial growth of monolayer WSe_2/graphene and non-epitaxial growth of MoS_2/graphene heterostructures, indicating the important role of the synthesis route on the microstructure of the resulting heterostructure. Ultra-high-resolution aberration-corrected STEM confirms growth of the single-layer WSe_2 and MoS_2 triangles with metal-terminated edges, while PL measurements show a significant photoluminescence quenching of TMDs on suspended graphene. In addition, this work shows the important role of the defects as the nucleation sites in the heterostructure growth. Such a technique will serve as a way to probe the competing mechanisms that derive nucleation and growth of a wide spectrum of heterolayers, further leading to nanoengineering of novel heterostructure devices.

EXPERIMENTAL SECTION

Graphene Growth and Transfer to the TEM Grid. Graphene film was grown on a Cu substrate using a chemical vapor deposition method.[1] The synthesized graphene film was then directly transferred from the Cu substrate to a gold Quantifoil TEM grid with 2 μm holes (Electron Microscopy Sciences).[28] The TEM grids were placed on the graphene/Cu substrate, and a drop of isopropyl alcohol was used to bring the graphene film into contact with the amorphous carbon on the grid. Sodium persulfate aqueous solution (0.2 g/mL) was then used to etch the Cu substrate. Following complete etching of Cu, the samples were moved to a distilled water bath to remove residual copper etchant.

Direct Growth of WSe_2 on Freestanding Graphene. The Au TEM grids covered with CVD graphene film were loaded into a MOCVD system. WSe_2 triangles were grown on freestanding graphene using hydrogen ambient at a pressure of 700 Torr and total flow of 100 sccm using Se/W ratios varying from 600 to 14 000. Tungsten hexacarbonyl ($W(CO)_6$) and dimethylselenide (DMSe) were used as the tungsten and selenium precursors, respectively. Growth occurred at temperatures between 800 and 850 °C at a ramp rate of 80 °C per minute for growth times of 30 min.

Direct Growth of MoS_2 on Freestanding Graphene. The MoS_2 was grown on the graphene TEM grids using oxide powder vaporization. Two milligrams of MoO_3 powder (Simga Aldrich 99.99%) was placed in an alumina crucible at the center of the furnace, where the temperature could reach ~750 °C. Then, 650 mg of sulfur powder (Alfa 99.9995%) was loaded into a fused crucible ($T \sim 200$ °C). The furnace was heated to 300 °C for 30 min in vacuum in order to remove all of the humidity, followed by ramping up to 750 °C for the growth. The growth was done for 10 min at 710 Torr and then the furnace cooled naturally. Ar (400 sccm) was used as the carrier gas during the experiment. As shown in Figure S3a, the graphene TEM grid was held by a 1 cm^2 sapphire that was placed 10 mm away from the powder.

Characterization of the Heterostructures. (S)TEM and EDS were utilized to study the atomic and chemical structure of WSe_2 and its epitaxy with respect to graphene. A JEOL 2010F S/TEM at 200 kV and a FEI Titan^3 60−300 S/TEM at 80 kV, both at Penn State, were used for this study. The beam current of 48 pA was used for the acquisition of HAADF-STEM images. The WSe_2/graphene and MoS_2/graphene heterostructures were characterized using Raman spectroscopy and photoluminescence with a WiTEC confocal Raman system. A 0.4 mW, 633 nm laser was used for the WSe_2/graphene samples, while a 0.5 mW, 488 nm laser was employed for the MoS_2/graphene heterostructures. The low powers were utilized in order to avoid sample damage in the freestanding heterostructures. The integration time of 10 s was used.

Conflict of Interest: The authors declare no competing financial interest.

Acknowledgment. A.A. and N.A. acknowledge support from NSF under EFRI 2-DARE Grant 1433378. A.A., N.A., S.E., and J.A.R. acknowledge the Center for 2-Dimensional and Layered Materials (2DLM) at the Pennsylvania State University. S.E., L.H., A.P., and J.A.R. acknowledge support from the Center for Low Energy Systems Technology (LEAST), one of six centers supported by the STARnet phase of the Focus Center Research Program (FCRP), a Semiconductor Research Corporation program sponsored by MARCO and DARPA. Authors would like to also acknowledge Dr. Takahira Miyagi, Mohammed Abu AlSaud, and Dixiong Wang for their help with graphene growth.

Supporting Information Available: Growth details and characterization of the WSe_2 and MoS_2 on EG and sapphire samples. This material is available free of charge *via* the Internet at http://pubs.acs.org.

REFERENCES AND NOTES

1. Li, X.; Cai, W.; An, J.; Kim, S.; Nah, J.; Yang, D.; Piner, R.; Velamakanni, A.; Jung, I.; Tutuc, E.; et al. Large-Area Synthesis of High-Quality and Uniform Graphene Films on Copper Foils. *Science* **2009**, *324*, 1312–1314.
2. Butler, S. Z.; Hollen, S. M.; Cao, L.; Cui, Y.; Gupta, J. A.; Gutiérrez, H. R.; Heinz, T. F.; Hong, S. S.; Huang, J.; Ismach, A. F.; et al. Progress, Challenges, and Opportunities in Two-Dimensional Materials Beyond Graphene. *ACS Nano* **2013**, *7*, 2898–2926.
3. Gibb, A. L.; Alem, N.; Chen, J.; Erickson, K. J.; Ciston, J.; Gautam, A.; Linck, M.; Zettl, A. Atomic Resolution Imaging of Grain Boundary Defects in Monolayer Chemical Vapor Deposition-Grown Hexagonal Boron Nitride. *J. Am. Chem. Soc.* **2013**, *135*, 6758–6761.
4. Azizi, A.; Zou, X.; Ercius, P.; Zhang, Z.; Elías, A. L.; Perea-López, N.; Stone, G.; Terrones, M.; Yakobson, B. I.; Alem, N. Dislocation Motion and Grain Boundary Migration in Two-Dimensional Tungsten Disulphide. *Nat. Commun.* **2014**, *5*, 4867.
5. Geim, A. K.; Grigorieva, I. V. van der Waals Heterostructures. *Nature* **2013**, *499*, 419–25.
6. Wang, L.; Meric, I.; Huang, P. Y.; Gao, Q.; Gao, Y.; Tran, H.; Taniguchi, T.; Watanabe, K.; Campos, L. M.; Muller, D. A.; et al. One-Dimensional Electrical Contact to a Two-Dimensional Material. *Science* **2013**, *342*, 614–617.
7. Britnell, L.; Gorbachev, R. V.; Jalil, R.; Belle, B. D.; Schedin, F.; Mishchenko, A.; Georgiou, T.; Katsnelson, M. I.; Eaves, L.; Morozov, S. V.; et al. Field-Effect Tunneling Transistor Based on Vertical Graphene Heterostructures. *Science* **2012**, *335*, 947–950.
8. Georgiou, T.; Jalil, R.; Belle, B. D.; Britnell, L.; Gorbachev, R. V.; Morozov, S. V.; Kim, Y.-J.; Gholinia, A.; Haigh, S. J.; Makarovsky, O.; et al. Vertical Field-Effect Transistor Based on Graphene–WS_2 Heterostructures for Flexible and Transparent Electronics. *Nat. Nanotechnol.* **2013**, *8*, 100–103.
9. Liu, Z.; Song, L.; Zhao, S.; Huang, J.; Ma, L.; Zhang, J.; Lou, J.; Ajayan, P. M. Direct Growth of Graphene/Hexagonal Boron Nitride Stacked Layers. *Nano Lett.* **2011**, *11*, 2032–2037.
10. Lopez-Sanchez, O.; Alarcon Llado, E.; Koman, V.; Fontcuberta i Morral, A.; Radenovic, A.; Kis, A. Light Generation and Harvesting in a van der Waals Heterostructure. *ACS Nano* **2014**, *8*, 3042–3048.
11. Hunt, B.; Sanchez-Yamagishi, J. D.; Young, A. F.; Yankowitz, M.; LeRoy, B. J.; Watanabe, K.; Taniguchi, T.; Moon, P.; Koshino, M.; Jarillo-Herrero, P.; et al. Massive Dirac Fermions and Hofstadter Butterfly in a van der Waals Heterostructure. *Science* **2013**, *340*, 1427–1430.
12. Tsai, C.; Chan, K.; Abild-Pedersen, F.; Nørskov, J. K. Active Edge Sites in $MoSe_2$ and WSe_2 Catalysts for the Hydrogen Evolution Reaction: A Density Functional Study. *Phys. Chem. Chem. Phys.* **2014**, *16*, 13156–13164.
13. Hinnemann, B.; Moses, P. G.; Bonde, J.; Jørgensen, K. P.; Nielsen, J. H.; Horch, S.; Chorkendorff, I.; Nørskov, J. K. Biomimetic Hydrogen Evolution: MoS_2 Nanoparticles as Catalyst for Hydrogen Evolution. *J. Am. Chem. Soc.* **2005**, *127*, 5308–5309.
14. Wang, H.; Kong, D.; Johanes, P.; Cha, J. J.; Zheng, G.; Yan, K.; Liu, N.; Cui, Y. $MoSe_2$ and WSe_2 Nanofilms with Vertically Aligned Molecular Layers on Curved and Rough Surfaces. *Nano Lett.* **2013**, *13*, 3426–3433.
15. Jaramillo, T. F.; Jørgensen, K. P.; Bonde, J.; Nielsen, J. H.; Horch, S.; Chorkendorff, I. Identification of Active Edge Sites for Electrochemical H_2 Evolution from MoS_2 Nanocatalysts. *Science* **2007**, *317*, 100–102.
16. Hansen, L. P.; Ramasse, Q. M.; Kisielowski, C.; Brorson, M.; Johnson, E.; Topsøe, H.; Helveg, S. Atomic-Scale Edge Structures on Industrial-Style MoS_2 Nanocatalysts. *Angew. Chem., Int. Ed.* **2011**, *50*, 10153–10156.
17. Dean, C. R.; Young, A. F.; Meric, I.; Lee, C.; Wang, L.; Sorgenfrei, S.; Watanabe, K.; Taniguchi, T.; Kim, P.; Shepard, K. L.; et al. Boron Nitride Substrates for High-Quality Graphene Electronics. *Nat. Nanotechnol.* **2010**, *5*, 722–726.
18. Lee, C.-H.; Lee, G.-H.; van der Zande, A. M.; Chen, W.; Li, Y.; Han, M.; Cui, X.; Arefe, G.; Nuckolls, C.; Heinz, T. F.; et al. Atomically Thin p–n Junctions with van der Waals Heterointerfaces. *Nat. Nanotechnol.* **2014**, *9*, 676–681.
19. Larentis, S.; Tolsma, J. R.; Fallahazad, B.; Dillen, D. C.; Kim, K.; MacDonald, A. H.; Tutuc, E. Band Offset and Negative Compressibility in Graphene–MoS_2 Heterostructures. *Nano Lett.* **2014**, *14*, 2039–2045.
20. Choi, M. S.; Lee, G.-H.; Yu, Y.-J.; Lee, D.-Y.; Lee, S. H.; Kim, P.; Hone, J.; Yoo, W. J. Controlled Charge Trapping by Molybdenum Disulphide and Graphene in Ultrathin Heterostructured Memory Devices. *Nat. Commun.* **2013**, *4*, 1624.
21. Zhang, W.; Chuu, C.-P.; Huang, J.-K.; Chen, C.-H.; Tsai, M.-L.; Chang, Y.-H.; Liang, C.-T.; Chen, Y.-Z.; Chueh, Y.-L.; He, J.-H.; et al. Ultrahigh-Gain Photodetectors Based on Atomically Thin Graphene–MoS_2 Heterostructures. *Sci. Rep.* **2014**, *4*, 3826.
22. Shanmugam, M.; Jacobs-Gedrim, R.; Song, E. S.; Yu, B. Two-Dimensional Layered Semiconductor/Graphene Heterostructures for Solar Photovoltaic Applications. *Nanoscale* **2014**, *6*, 12682–12689.
23. Roy, T.; Tosun, M.; Kang, J. S.; Sachid, A. B.; Desai, S. B.; Hettick, M.; Hu, C. C.; Javey, A. Field-Effect Transistors Built from All Two-Dimensional Material Components. *ACS Nano* **2014**, *8*, 6259–6264.
24. Loan, P. T. K.; Zhang, W.; Lin, C.-T.; Wei, K.-H.; Li, L.-J.; Chen, C.-H. Graphene/MoS_2 Heterostructures for Ultrasensitive Detection of DNA Hybridisation. *Adv. Mater.* **2014**, *26*, 4838–4844.
25. Hui, Y. Y.; Liu, X.; Jie, W.; Chan, N. Y.; Hao, J.; Hsu, Y.-T.; Li, L.-J.; Guo, W.; Lau, S. P. Exceptional Tunability of Band Energy in a Compressively Strained Trilayer MoS_2 Sheet. *ACS Nano* **2013**, *7*, 7126–7131.
26. Lin, Y.-C.; Lu, N.; Perea-Lopez, N.; Li, J.; Lin, Z.; Peng, X.; Lee, C. H.; Sun, C.; Calderin, L.; Browning, P. N.; et al. Direct Synthesis of van der Waals Solids. *ACS Nano* **2014**, *8*, 3715–3723.
27. Shi, Y.; Zhou, W.; Lu, A.-Y.; Fang, W.; Lee, Y.-H.; Hsu, A. L.; Kim, S. M.; Kim, K. K.; Yang, H. Y.; Li, L.-J.; et al. van der Waals Epitaxy of MoS_2 Layers Using Graphene as Growth Templates. *Nano Lett.* **2012**, *12*, 2784–2791.
28. Regan, W.; Alem, N.; Alemán, B.; Geng, B.; Girit, C.; Maserati, L.; Wang, F.; Crommie, M.; Zettl, A. A Direct Transfer of Layer-Area Graphene. *Appl. Phys. Lett.* **2010**, *96*, 113102.
29. Eichfeld, S. M.; Eichfeld, C. M.; Lin, Y.-C.; Hossain, L.; Robinson, J. A. Rapid, Non-destructive Evaluation of Ultrathin WSe_2 Using Spectroscopic Ellipsometry. *APL Mater.* **2014**, *2*, 092508.
30. Najmaei, S.; Liu, Z.; Zhou, W.; Zou, X.; Shi, G.; Lei, S.; Yakobson, B. I.; Idrobo, J.-C.; Ajayan, P. M.; Lou, J. Vapour Phase Growth and Grain Boundary Structure of Molybdenum Disulphide Atomic Layers. *Nat. Mater.* **2013**, *12*, 754–759.
31. Alem, N.; Ramasse, Q. M.; Seabourne, C. R.; Yazyev, O. V.; Erickson, K.; Sarahan, M. C.; Kisielowski, C.; Scott, A. J.; Louie, S. G.; Zettl, A. Subangstrom Edge Relaxations Probed by

Electron Microscopy in Hexagonal Boron Nitride. *Phys. Rev. Lett.* **2012**, *109*, 205502.
32. Alem, N.; Yazyev, O. V.; Kisielowski, C.; Denes, P.; Dahmen, U.; Hartel, P.; Haider, M.; Bischoff, M.; Jiang, B.; Louie, S. G.; et al. Probing the Out-of-Plane Distortion of Single Point Defects in Atomically Thin Hexagonal Boron Nitride at the Picometer Scale. *Phys. Rev. Lett.* **2011**, *106*, 126102.
33. Koma, A. van der Waals Epitaxy—A New Epitaxial Growth Method for a Highly Lattice-Mismatched System. *Thin Solid Films* **1992**, *216*, 72–76.
34. Wilson, J. A.; Yoffe, A. D. The Transition Metal Dichalcogenides Discussion and Interpretation of the Observed Optical, Electrical and Structural Properties. *Adv. Phys.* **1969**, *18*, 193–335.
35. van der Zande, A. M.; Huang, P. Y.; Chenet, D. A.; Berkelbach, T. C.; You, Y.; Lee, G.-H.; Heinz, T. F.; Reichman, D. R.; Muller, D. A.; Hone, J. C. Grains and Grain Boundaries in Highly Crystalline Monolayer Molybdenum Disulphide. *Nat. Mater.* **2013**, *12*, 554–561.
36. Terrones, H.; Del Corro, E.; Feng, S.; Poumirol, J. M.; Rhodes, D.; Smirnov, D.; Pradhan, N. R.; Lin, Z.; Nguyen, M. A. T.; Elías, A. L.; et al. New First Order Raman-Active Modes in Few Layered Transition Metal Dichalcogenides. *Sci. Rep.* **2014**, *4*, 4215.
37. Li, H.; Lu, G.; Wang, Y.; Yin, Z.; Cong, C.; He, Q.; Wang, L.; Ding, F.; Yu, T.; Zhang, H. Mechanical Exfoliation and Characterization of Single- and Few-Layer Nanosheets of WSe_2, TaS_2, and $TaSe_2$. *Small* **2013**, *9*, 1974–1981.
38. Calderon, H. A.; Kisielowski, C.; Specht, P.; Barton, B.; Godinez-Salomon, F.; Solorza-Feria, O. Maintaining the Genuine Structure of 2D Materials and Catalytic Nanoparticles at Atomic Resolution. *Micron* **2015**, *68*, 164–175.
39. Zhu, Y.; Ramasse, Q. M.; Brorson, M.; Moses, P. G.; Hansen, L. P.; Kisielowski, C. F.; Helveg, S. Visualizing the Stoichiometry of Industrial-Style Co-Mo-S Catalysts with Single-Atom Sensitivity. *Angew. Chem., Int. Ed.* **2014**, *53*, 10723–10727.
40. Lee, Y.-H.; Zhang, X.-Q.; Zhang, W.; Chang, M.-T.; Lin, C.-T.; Chang, K.-D.; Yu, Y.-C.; Wang, J. T.-W.; Chang, C.-S.; Li, L.-J.; et al. Synthesis of Large-Area MoS_2 Atomic Layers with Chemical Vapor Deposition. *Adv. Mater.* **2012**, *24*, 2320–2325.
41. Hollander, M. J.; Agrawal, A.; Bresnehan, M. S.; LaBella, M.; Trumbull, K. A.; Cavalero, R.; Snyder, D. W.; Datta, S.; Robinson, J. A. Heterogeneous Integration of Hexagonal Boron Nitride on Bilayer Quasi-Free-Standing Epitaxial Graphene and Its Impact on Electrical Transport Properties. *Phys. Status Solidi* **2013**, *210*, 1062–1070.
42. Konar, A.; Fang, T.; Jena, D. Effect of High-κ Gate Dielectrics on Charge Transport in Graphene-Based Field Effect Transistors. *Phys. Rev. B* **2010**, *82*, 115452.